

EXTREME EMISSION LINE GALAXIES IN CANDELS: BROAD-BAND SELECTED, STAR-BURSTING DWARF GALAXIES AT $Z > 1$

A. VAN DER WEL¹, A. N. STRAUGHN², H.-W. RIX¹, S. L. FINKELSTEIN³, A. M. KOEKEMOER⁴, B. J. WEINER⁵, S. WUYTS⁶, E. F. BELL⁷, S. M. FABER⁸, J. R. TRUMP⁸, D. KOO⁸, H. C. FERGUSON⁴, C. SCARLATA⁹, N. P. HATHI¹⁰, J. S. DUNLOP¹¹, J. A. NEWMAN¹², M. DICKINSON¹³, B. W. SALMON³, D. F. DE MELLO^{14,15}, D. D. KOCEVSKI⁸, K. LAI⁸, N. A. GROGIN⁴, S. A. RODNEY¹⁶, YICHENG GUO¹⁷, E. G. MCGRATH⁸, K.-S. LEE¹⁸, G. B. CALVO⁸, K.-H. HUANG¹⁶

Version: July 27, 2011

ABSTRACT

We identify an abundant population of extreme emission line galaxies (EELGs) at redshift $z = 1.6 - 1.8$ in the Cosmic Assembly Near-IR Deep Extragalactic Legacy Survey (CANDELS) imaging from *Hubble Space Telescope/Wide Field Camera 3* (HST/WFC3). 69 EELG candidates are selected by the large contribution of exceptionally bright emission lines to their near-infrared, broad-band fluxes. Supported by spectroscopic confirmation of strong [OIII] emission lines – with rest-frame equivalent widths $\sim 1000\text{\AA}$ – in the four candidates that have HST/WFC3 grism observations, we conclude that these objects are dwarf galaxies with $\sim 10^8 M_{\odot}$ in stellar mass, undergoing an enormous starburst phase with M_*/\dot{M}_* of only ~ 15 Myr. These bursts may cause outflows that are strong enough to produce cored dark matter profiles in low-mass galaxies. The individual star formation rates and the co-moving number density ($3.7 \times 10^{-4} \text{ Mpc}^{-3}$) can produce in ~ 4 Gyr much of the stellar mass density that is presently contained in $10^8 - 10^9 M_{\odot}$ dwarf galaxies. Therefore, our observations provide a strong indication that many or even most of the stars in present-day dwarf galaxies formed in strong, short-lived bursts, mostly at $z > 1$.

1. INTRODUCTION

The formation history of dwarf galaxies with masses $\sim 10^8 M_{\odot}$ can usually only be studied through ‘archaeological’ age reconstruction, based on resolved stel-

lar populations (e.g., Grebel 1997; Mateo 1998). Their high-redshift progenitors have so far remained elusive despite the ever increasing depth of spectroscopic observing campaigns and imaging from the ground and the *Hubble Space Telescope* (HST). In this Letter we identify an abundant population of $z > 1$ dwarf galaxies undergoing extreme starbursts, through HST/*Wide Field Camera 3* (WFC3) imaging from the Cosmic Assembly Near-IR Deep Extragalactic Legacy Survey (CANDELS, Grogin et al. 2011; Koekemoer et al. 2011), that may well be the progenitors of present-day dwarf galaxies with stellar masses $\sim 10^8 - 10^9 M_{\odot}$.

At the present day, starbursts contribute a minority to the total star formation activity in dwarf galaxies (Lee et al. 2009). However, there is abundant evidence that the star formation histories are complex and that bursts play an important role (as reviewed by Mateo 1998). Many authors find evidence for short-lived (~ 10 Myr) SF events in nearby star-forming dwarf galaxies from a range of observational and modeling techniques (e.g., Schaerer et al. 1999; Mas-Hesse & Kunth 1999; Thornley et al. 2000; Tremonti et al. 2001; Harris et al. 2004), while others argue that star formation epochs are more prolonged (e.g., Calzetti et al. 1997; Lee 2008; McQuinn et al. 2009). Simulations also indicate that star formation histories of low-mass galaxies are episodic or even burst-like (e.g., Pelupessy et al. 2004; Nagamine 2010).

As most stars in dwarf galaxies formed more than 5 Gyr ago (e.g., Dolphin et al. 2005; Weisz et al. 2011), it is crucial to understand the mode of star formation in dwarf galaxies at those early epochs, but ‘archaeological’ studies do not have the resolution in terms of stellar population age to constrain strengths, durations, and frequency of bursts. The increased frequency of interaction

¹ Max-Planck Institut für Astronomie, Königstuhl 17, D-69117, Heidelberg, Germany; e-mail:vdwel@mpia.de

² Astrophysics Science Division, Goddard Space Flight Center, Code 665, Greenbelt, MD 20771, USA

³ George P. and Cynthia Woods Mitchell Institute for Fundamental Physics and Astronomy, Department of Physics & Astronomy, Texas A&M University, College Station, TX 77843, USA

⁴ Space Telescope Science Institute, 3700 San Martin Drive, Baltimore, MD 21218, USA

⁵ Steward Observatory, 933 N. Cherry St., University of Arizona, Tucson, AZ 85721, USA

⁶ Max-Planck-Institut für Extraterrestrische Physik, Giessenbachstrasse, D-85748 Garching, Germany

⁷ Department of Astronomy, University of Michigan, 500 Church Street, Ann Arbor, Michigan, 48109, USA

⁸ University of California Observatories/Lick Observatory, University of California, Santa Cruz, CA 95064, USA

⁹ Minnesota Institute for Astrophysics, University of Minnesota, 116 Church St. S.E. Minneapolis, MN 55455, USA

¹⁰ Observatories of the Carnegie Institution of Washington, Pasadena, CA 91101, USA

¹¹ Institute for Astronomy, University of Edinburgh, Royal Observatory, Edinburgh EH9 3HJ, UK

¹² Department of Physics and Astronomy, University of Pittsburgh, 3941 O’Hara Street, Pittsburgh, PA 15260, USA

¹³ National Optical Astronomy Observatory, 950 North Cherry Avenue, Tucson, AZ 85719, USA

¹⁴ Department of Physics, The Catholic University of America, Washington DC 20064, USA

¹⁵ Observational Cosmology Laboratory, Goddard Space Flight Center, Code 665, Greenbelt, MD 20771, USA

¹⁶ Department of Physics and Astronomy, Johns Hopkins University, Baltimore, MD 21218, USA

¹⁷ Astronomy Department, University of Massachusetts, 710 N. Pleasant Street, Amherst, MA 01003, USA

¹⁸ Yale Center for Astronomy and Astrophysics, 260 Whitney Avenue, JWG 454 New Haven, CT 06511, USA

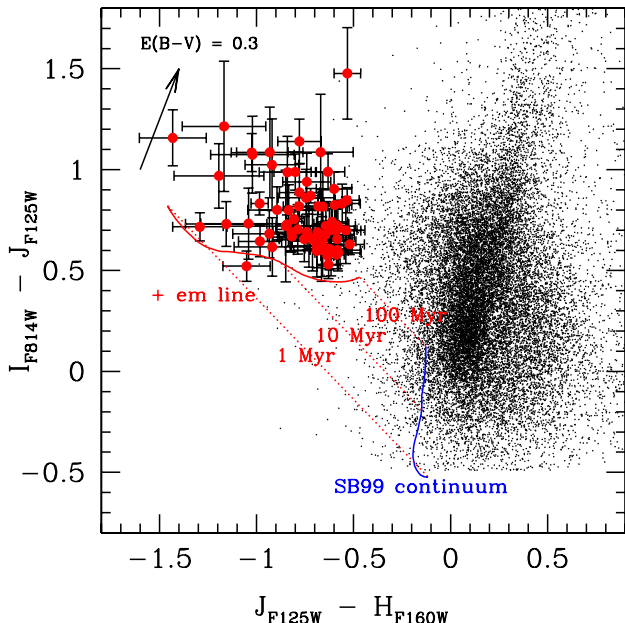


Figure 1. Observed $I -$ vs. $J -$ colors (in AB magnitudes) from HST/WFC3 and ACS imaging for all objects in the UDS and GSD (small black points) and the sample of emission-line dominated objects (large red points with error bars), selected by $I - > 0.44 + \sigma(I -)$ and $J - < -0.44 - \sigma(J -)$, where $\sigma(I -)$ and $\sigma(J -)$ are the 1 errors on the colors. The blue line represents the redshifted ($z \sim 1.5$) continuum colors of the Starburst99 model (Leitherer et al. 1999) for continuous star formation, in the age range from 1 Myr to 100 Myr as indicated by the red labels. The red line represents the same model, but with the J-band flux increased by the emission line luminosity predicted by the model (Starburst99 predicts $H\alpha$ luminosity \sim [OIII] emission, which affects the J band at this redshift, is approximately equally luminosity for low-metallicity starbursts). The model tracks merely serve to illustrate that the deviant colors of the selected objects can be explained by the contribution of a bright emission line to the J band flux. The black arrow indicates dust attenuation.

with other galaxies and higher gas fractions at $z > 1$ may have resulted in strong, short-lived starbursts. In this Letter we address the open question of how many and how frequently strong, short-lived starbursts occur in dwarf galaxies at $z > 1$, and how relevant this mode of star formation is for the build-up of the dwarf galaxy population in a cosmological context.

2. DATA

2.1. Multi-Wavelength Imaging

We select objects from multi-wavelength photometry of two fields with HST/WFC3 and *Advanced Camera for Surveys* (ACS) coverage: the Ultra Deep Survey (UDS) field and the GOODS-South Deep (GSD) field at 4-epoch depth.¹⁹ For the UDS we use WFC3 imaging in F125W (J) and F160W (H) and ACS imaging in F814W (I) from CANDELS. For the GSD we use the J and H band imaging from CANDELS, amended by WFC3 imaging from the Early Release Science (ERS) program (Windhorst et al. 2011), and I band imaging

¹⁹ GOODS is the Great Observatories Origins Deep Survey. CANDELS provides deep images over the central parts of GOODS-North and GOODS-South, and wider, less deep imaging over the remainder of those fields and over the other CANDELS fields, including UDS. See the CANDELS website, <http://candels.uchicago.edu/>, for details of the field layouts.

from GOODS (Giavalisco et al. 2004). The total area with I -, J -, and H -band coverage used here is 279 square arcminutes.

Sources are detected in the H band with SExtractor (Bertin & Arnouts 1996) and photometry is performed with TFIT (Laidler et al. 2007), which uses additional imaging data sets, ranging from U to $4.5\mu\text{m}$ to produce resolution-matched, multi-wavelength catalogs. The catalog construction is described in full by Guo et al. (in prep.). In addition, we use a version of GALAPAGOS (Häussler et al. 2007) adapted for CANDELS WFC3 imaging to measure structural parameters (van der Wel et al., in prep.).

2.2. Color-Color Selection

We select objects that are red in $I - J$ and blue in $J - H$ (see Figure 1), tracing luminous emission lines that contribute significantly to the total J -band light. No known continuum emission can produce such broadband colors. The highlighted objects in Figure 1 have $I - J > 0.44 + \sigma(I - J)$ and $J - H < -0.44 - \sigma(J - H)$, where σ refers to the color uncertainty; that is, we select those objects that are significantly more than 50% brighter in J than in both I and H . We identify 69 such objects. They range in magnitude from $H_{\text{AB}} = 24$ to $H_{\text{AB}} = 27$, with a median of $H = 25.8$ (see Table 1). We note that there is no gap in color-color space between the emission line galaxy candidates that we select and the general distribution; the selected objects are merely the most extreme outliers.

In Figure 2 we show false-color composites of all 69 candidates. These sources are typically compact, but not point sources; their J - and H -band half-light radii from GALFIT are typically $0.1''$. A subset ($\sim 20\%$) are more extended or consist of multiple components. We show the U through $4.5\mu\text{m}$ spectral energy distributions (SEDs) of a subset of the emission-line candidates in Figure 3. The SEDs are seen to be almost entirely flat in F_ν , or in terms of ultra-violet spectral slope they have $\beta \sim -2$, where β is defined as $F_\lambda = \lambda^\beta$. The J band is a notable outlier from this SED shape for all these objects.

3. EXTREMELY BRIGHT EMISSION LINES

3.1. Photometric Constraints

No known objects have continuum SEDs that resemble those shown in Figure 3. Our hypothesis is that the J -band excess is due to one or more emission lines. The implied equivalent widths in the observed frame are extraordinarily high: $\text{EW} \sim 1500 - 3000\text{\AA}$.

Among the emission lines that can reach such extreme EWs, $\text{Ly}\alpha$ and [OII] are immediately ruled out because the implied high redshift would produce an observed break in, at least, the U band; the lack of such a break implies $z < 2$ for these objects. WFC3/UVIS observations (Windhorst et al. 2011) provide UV photometry over the ERS area. The average color of those candidates in the ERS area is $F_{275W} - U = 1.44$, which suggests that the Lyman break is situated at around 3000\AA , which, in combination with the very blue continuum slopes redward of the U band, implies $z > 1.5$. Only one candidate with UVIS coverage has a $F_{275W} - U$ color consistent with that of a galaxy at $z < 1.5$. The implication is that strong [OIII] emission at 4959\AA and 5007\AA provide the

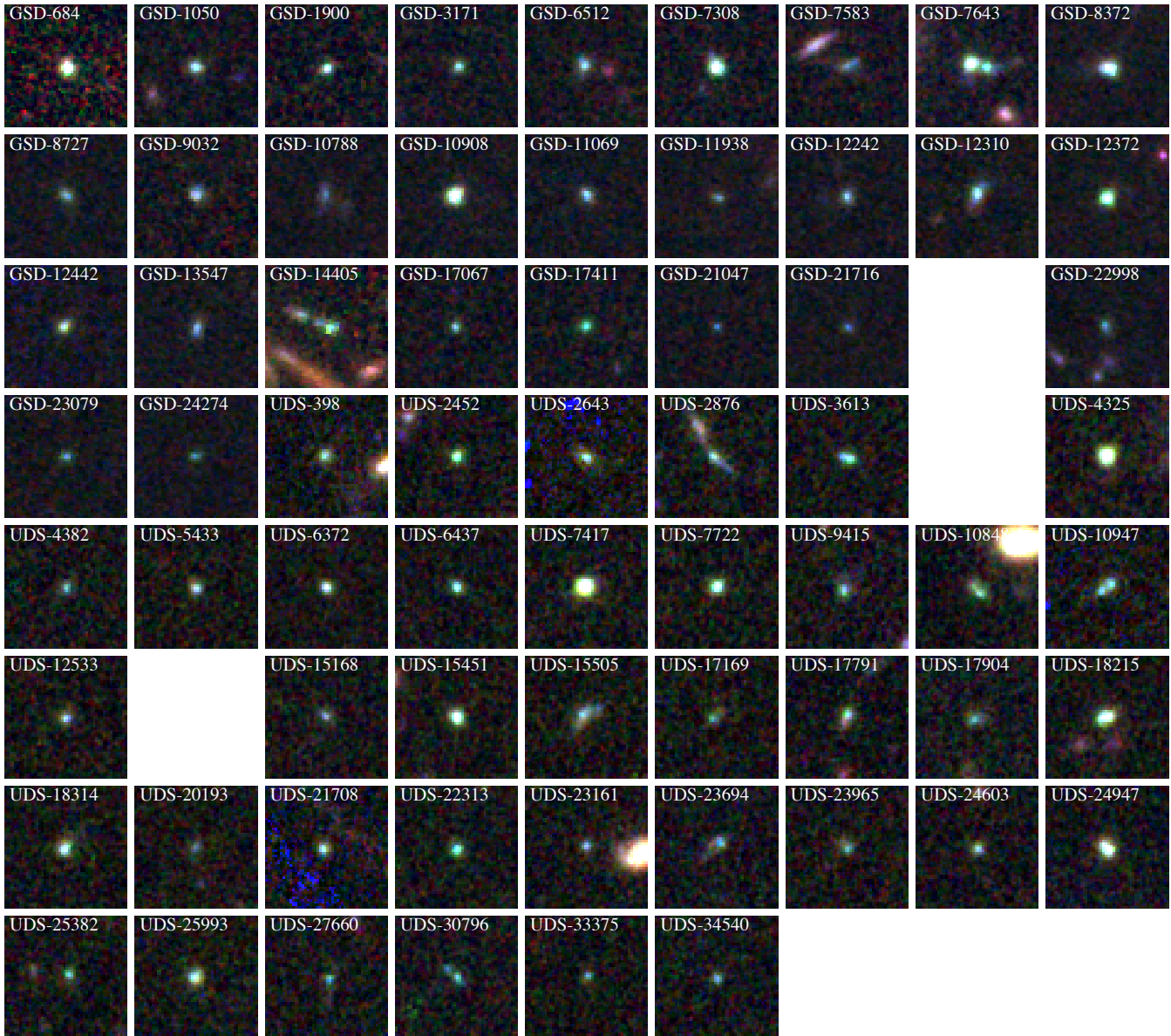


Figure 2. False-color composites, created from HST I, J, and H band image cutouts ($3''$ on a side), of the 69 emission line galaxy candidates. The IDs correspond to those in Table 1. The sources are typically compact, although a subset of about 20% have more extended morphologies or feature multiple components.

most plausible explanation for the J band excess light.

If [OIII] is responsible for the J band excess the redshift upper limit is $z = 1.8$. Furthermore, because we select objects with blue $J - H$ colors, the H cannot contain the bright $H\alpha$ line, which implies $z > 1.6$. Thus, solely based on their photometric properties, we suggest that our candidates are strong [OIII] emitters in the redshift range $1.6 < z < 1.8$.

3.2. Spectroscopic Constraints

The hypothesis that [OIII] emission at $z \sim 1.7$ explains the J band excess light is strongly supported by spectroscopic observations. While none of the candidates have ground-based spectra, WFC3 grism observations are available for small portions of the GSD (one pointing in the ERS field, Straughn et al. 2011) and the UDS (from CANDELS, Weiner et al. , in prep.). The available grism coverage overlaps with the positions of 4

candidates in our sample (1 in the ERS, 3 in the UDS), and strong emission lines are detected in all 4 cases. The spectra (Figure 4) all show bright emission lines in the wavelength range $1.3 - 1.4 \mu m$, whose combined fluxes are in agreement with the excess light seen in the J band.

The lines in all 4 spectra are readily identified as [OIII]: the asymmetry of the bright line, always extended blueward, is due to the two components of the [OIII] line, at 5007\AA and at 4959\AA , where the latter is $\sim 3\times$ fainter. In all cases, $H\beta$ is also detected. The redshifts are all in the range $z = 1.65 - 1.80$, in excellent agreement with what we inferred solely from photometry. We conclude that our sample of extreme emission line galaxies (EELGs) form the high-EW tail of the general population of emission line galaxies seen in ACS and WFC3 spectroscopic grism observations (e.g., Straughn et al. 2008, 2009; Atek et al. 2010; Straughn et al. 2011).

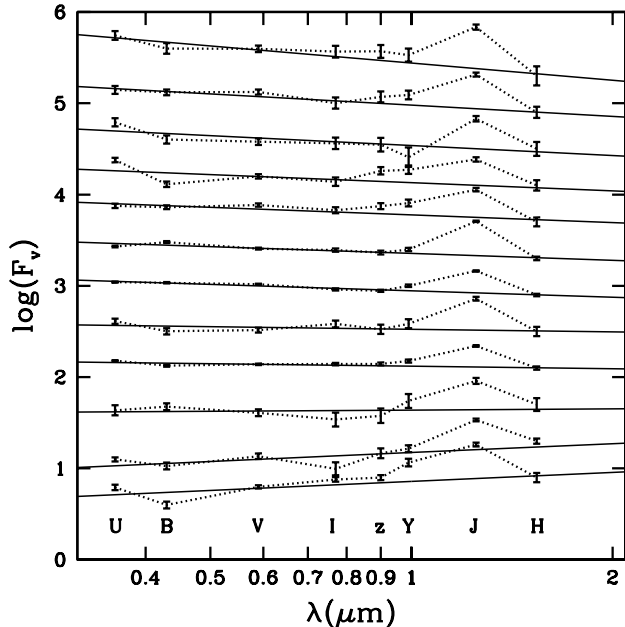


Figure 3. Broad-band SEDs of the 12 emission line galaxy candidates selected from the GSD field. Units on the y-axis are arbitrary, and the SEDs are incrementally offset by 0.4 dex in the vertical direction for clarity, sorted by continuum slope, indicated by the solid lines, with the bluest at the top. The objects are characterized by flat SEDs in F_ν over the entire range from U band to H band, consistent with those of very young stellar populations with ages < 50 Myr. The J band noticeably deviates from this trend as the result of strong emission line contributions. Among the lines that can physically have such large luminosities, Ly α and [OII] are ruled out based on the bright U and B band fluxes, restricting the possible redshift range to $z < 2$. If H α causes the excess J-band flux, then [OIII] is expected to produce a similar excess in the I, z, or Y band, which is not observed. The most likely explanation for the excess J-band flux is the [OIII] nebular emission line, which is consistent with all other broad-band colors as long as the objects are in the redshift range $1.6 < z < 1.8$.

3.3. Emission Lines and Broad-Band Photometry

The existence of such strong [OIII] emitters has been demonstrated before. At low redshifts, $z < 0.4$, Cardamone et al. (2009) identified a rare class of emission-line dominated objects through broad-band colors. Narrow-band surveys identified galaxies with strong [OIII] and H α emission lines with $EW \sim 100 - 1000 \text{ \AA}$ at redshifts $z = 0.3 - 1$ (e.g., Kakazu et al. 2007), demonstrated to be young and metal poor (Hu et al. 2009). Most notably, Atek et al. (2010) identified galaxies with [OIII] emission lines with $EW > 1000 \text{ \AA}$ at $z = 1 - 1.5$; these objects are likely of the same nature as those in our broad-band selected sample.

We have shown that selecting objects which are much brighter in J than in I and H works as a rather clean method for finding strong [OIII] emitters at $1.6 < z < 1.8$. Emission line galaxies with such excesses in other bands also exist, but a systematic search is more complicated as at most redshift ranges, multiple lines (most notably [OIII] and H α) affect multiple photometric bands. Therefore, we refrain from conducting such a systematic search here.

The existence of such emission-line dominated galaxies complicates the interpretation of SEDs, which is especially relevant in the case of the search for and SED

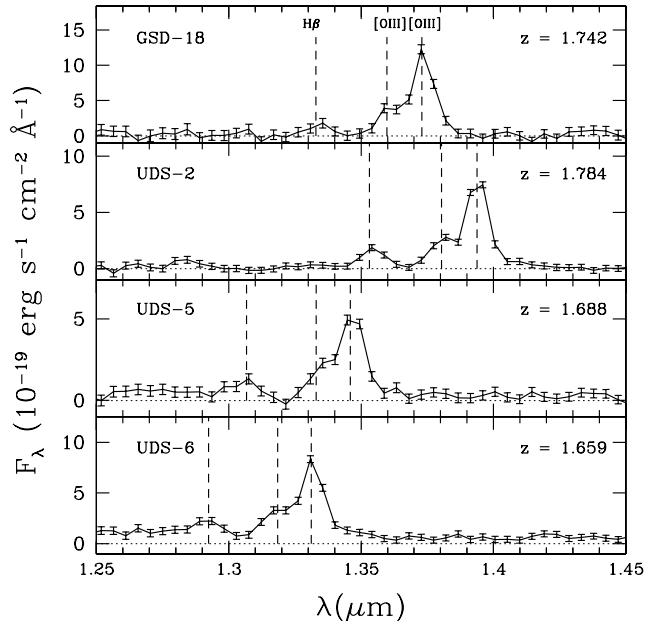


Figure 4. WFC3 grism spectra of the four candidates with grism coverage. The IDs refer to those in Table 1. GSD-18 is object 402 from Straughn et al. (2011); the 3 objects in the UDS are from CANDELS grism observations (Weiner et al., in prep.). All spectra unambiguously demonstrate that [OIII] emission explains the large excess J-band flux: H β is clearly detected in most cases, the brightest line is clearly asymmetric in all cases due to the blended 5007 \AA and 4959 \AA components of [OIII] (the latter is ~ 3 times weaker). The combined fluxes of the emission lines corresponds well to the magnitude difference between J and H in all cases. These spectra strongly suggest that the majority of the objects in our sample are [OIII] emitters at $z \sim 1.7$.

modeling of rare, high-redshift objects. Although contamination by emission lines is often considered to be a factor (e.g., Labbé et al. 2010), the extremely bright lines we observe suggests that their effect may be underestimated. Ono et al. (2010) explicitly showed that red colors in Ly α emitters and $z = 7$ Lyman break galaxies may indicate the presence of evolved stellar populations or strong nebular emission lines (also see Schaerer et al. 1999; Finkelstein et al. 2011). Steep UV continuum slopes, such as observed in our objects, should serve as a warning sign for contamination by nebular emission lines at longer wavelengths to the point that those can dominate the broad-band flux.

4. STARBURSTING DWARF GALAXIES AT $Z = 1.7$

4.1. Star formation or AGN?

Before turning to our preferred starburst interpretation, let us first point out that nuclear activity is not a likely explanation for the bright emission lines in the vast majority of EELGs. None of the objects in the CDFS have significant detections in X-ray or at $24 \mu\text{m}$, and the objects are spatially resolved in both J and H.

Moreover, it is highly unlikely that all 69 objects are dominated by line emission from active galactic nuclei. At least at the present day, low-mass, low-metallicity AGN are exceedingly rare (Izotov & Thuan 2008), much rarer than starbursting dwarf galaxies (Izotov et al. 2011). The implied black hole masses for the objects in our sample, as inferred from their UV continuum luminosities (Shen et al. 2008) are $\sim 10^6 M_\odot$ at

Table 1
Sample of Extreme Emission Line Galaxies

ID	RA (deg)	DEC (deg)	H (AB)	EW _{OIII,5007} (Å)	2500	log (M) (M _⊙)
GSD-1	53.1670647	-27.8589363	24.67 ± 0.07	459 ± 40	-1.83 ± 0.09	8.57 ± 0.17
GSD-2	53.0803452	-27.8505726	25.63 ± 0.07	569 ± 67	-2.04 ± 0.19	7.96 ± 0.19
GSD-3	53.0460205	-27.8373222	25.88 ± 0.11	507 ± 75	-2.02 ± 0.18	7.94 ± 0.20
GSD-4	53.1050873	-27.8199749	26.20 ± 0.11	769 ± 143	-1.75 ± 0.30	7.72 ± 0.22
GSD-5	53.0675087	-27.7735958	25.05 ± 0.08	566 ± 74	-2.19 ± 0.19	8.14 ± 0.19
GSD-6	53.0974998	-27.7639198	24.99 ± 0.05	700 ± 53	-2.12 ± 0.09	8.10 ± 0.17
GSD-7	53.1221275	-27.7595425	25.44 ± 0.12	535 ± 99	-1.70 ± 0.28	8.20 ± 0.22
GSD-8	53.1719360	-27.7591457	24.26 ± 0.04	693 ± 47	-1.76 ± 0.11	8.52 ± 0.17
GSD-9	53.0787544	-27.7502880	24.86 ± 0.04	468 ± 32	-1.99 ± 0.10	8.42 ± 0.17
GSD-10	53.0636902	-27.7458534	26.37 ± 0.09	759 ± 134	-1.56 ± 0.33	7.72 ± 0.22
GSD-11	53.0074997	-27.7418671	25.97 ± 0.09	534 ± 76	-2.13 ± 0.19	7.84 ± 0.20
GSD-12	53.1146126	-27.7219791	25.80 ± 0.12	641 ± 139	-1.94 ± 0.31	7.87 ± 0.23
GSD-13	53.1015167	-27.7208824	24.77 ± 0.03	490 ± 29	-2.35 ± 0.08	8.29 ± 0.16
GSD-14	53.0559082	-27.7188034	26.00 ± 0.08	501 ± 65	-1.90 ± 0.20	7.94 ± 0.19
GSD-15	53.1495361	-27.7102852	26.64 ± 0.15	820 ± 288	-2.20 ± 0.57	7.36 ± 0.30
GSD-16	53.1476173	-27.7070885	26.10 ± 0.08	582 ± 80	-2.08 ± 0.22	7.75 ± 0.20
GSD-17	53.0642204	-27.7065239	25.41 ± 0.05	465 ± 43	-2.20 ± 0.13	8.12 ± 0.17
GSD-18	53.0712929	-27.7058029	25.24 ± 0.04	861 ± 66	-2.36 ± 0.11	7.85 ± 0.17
GSD-19	53.1819763	-27.7050381	25.71 ± 0.06	1002 ± 245	-2.18 ± 0.41	7.72 ± 0.23
GSD-20	53.1408157	-27.6923904	26.23 ± 0.10	496 ± 82	-1.83 ± 0.26	7.88 ± 0.21
GSD-21	53.1009369	-27.6767044	24.76 ± 0.10	935 ± 139	-0.95 ± 0.28	8.54 ± 0.21
GSD-22	53.1184502	-27.8199196	26.76 ± 0.13	870 ± 198	-1.88 ± 0.36	7.41 ± 0.24
GSD-23	53.0776062	-27.8127956	26.81 ± 0.17	1512 ± 338	-2.22 ± 0.28	7.30 ± 0.25
GSD-24	53.1329727	-27.7401028	27.77 ± 0.30	698 ± 318	-2.23 ± 0.47	6.95 ± 0.38
GSD-25	53.0843887	-27.7279205	27.29 ± 0.15	562 ± 164	-2.39 ± 0.43	7.18 ± 0.27
GSD-26	53.1415024	-27.7248802	26.65 ± 0.10	650 ± 106	-2.10 ± 0.25	7.47 ± 0.21
GSD-27	53.1125793	-27.7070904	26.91 ± 0.13	954 ± 262	-2.40 ± 0.42	7.15 ± 0.26
GSD-28	53.0461197	-27.7056046	27.13 ± 0.16	1009 ± 293	-2.14 ± 0.45	7.16 ± 0.28
GSD-29	53.1399536	-27.6751385	27.79 ± 0.21	1314 ± 557	-2.12 ± 0.74	6.93 ± 0.37
UDS-1	34.2752991	-5.2744966	25.38 ± 0.09	576 ± 90	-1.33 ± 0.18	8.31 ± 0.20
UDS-2	34.4407692	-5.2625666	25.74 ± 0.09	1081 ± 147	-1.41 ± 0.17	7.99 ± 0.20
UDS-3	34.4821739	-5.2613993	25.28 ± 0.08	507 ± 95	-1.88 ± 0.24	8.23 ± 0.20
UDS-4	34.2686577	-5.2600641	25.44 ± 0.10	614 ± 83	-1.53 ± 0.14	8.18 ± 0.19
UDS-5	34.4264832	-5.2557702	25.69 ± 0.11	701 ± 95	-1.66 ± 0.10	7.99 ± 0.20
UDS-6	34.4285698	-5.2553182	25.10 ± 0.07	731 ± 86	-2.12 ± 0.13	8.04 ± 0.18
UDS-7	34.3256760	-5.2517433	24.32 ± 0.04	656 ± 43	-1.59 ± 0.05	8.58 ± 0.17
UDS-8	34.3140144	-5.2510471	26.44 ± 0.17	728 ± 153	-1.39 ± 0.20	7.77 ± 0.24
UDS-9	34.3825874	-5.2446208	25.94 ± 0.09	478 ± 64	-1.82 ± 0.14	8.03 ± 0.19
UDS-10	34.2635345	-5.2394333	25.48 ± 0.07	541 ± 64	-1.84 ± 0.14	8.13 ± 0.18
UDS-11	34.3112793	-5.2389579	26.36 ± 0.10	735 ± 94	-2.43 ± 0.12	7.42 ± 0.19
UDS-12	34.4738884	-5.2342329	24.15 ± 0.03	713 ± 42	-1.72 ± 0.05	8.57 ± 0.16
UDS-13	34.3181419	-5.2322998	25.35 ± 0.07	716 ± 68	-2.12 ± 0.08	7.95 ± 0.18
UDS-14	34.4815674	-5.2224994	25.69 ± 0.11	602 ± 96	-2.30 ± 0.15	7.81 ± 0.20
UDS-15	34.3711662	-5.2148032	25.45 ± 0.09	843 ± 111	-1.35 ± 0.15	8.14 ± 0.19
UDS-16	34.4829216	-5.2141871	25.39 ± 0.08	662 ± 87	-1.80 ± 0.15	8.07 ± 0.19
UDS-17	34.2475166	-5.2053304	25.95 ± 0.10	469 ± 63	-2.22 ± 0.13	7.89 ± 0.19
UDS-18	34.3154488	-5.2009025	25.83 ± 0.13	739 ± 136	-1.87 ± 0.17	7.84 ± 0.21
UDS-19	34.2988663	-5.1918006	26.25 ± 0.15	543 ± 106	-1.94 ± 0.17	7.79 ± 0.23
UDS-20	34.2320824	-5.1903882	25.16 ± 0.06	648 ± 55	-2.20 ± 0.06	8.03 ± 0.17
UDS-21	34.3089409	-5.1900907	25.15 ± 0.07	609 ± 66	-2.28 ± 0.11	8.03 ± 0.18
UDS-22	34.4167404	-5.1804438	26.34 ± 0.19	1070 ± 307	-1.72 ± 0.31	7.64 ± 0.28
UDS-23	34.3870239	-5.1772404	25.59 ± 0.07	591 ± 74	-2.15 ± 0.14	7.91 ± 0.18
UDS-24	34.2528458	-5.1763620	26.02 ± 0.13	779 ± 140	-1.40 ± 0.19	7.91 ± 0.22
UDS-25	34.4021454	-5.1753521	24.47 ± 0.05	507 ± 39	-2.11 ± 0.06	8.48 ± 0.17
UDS-26	34.4591904	-5.1744485	25.34 ± 0.08	552 ± 59	-2.29 ± 0.09	8.01 ± 0.18
UDS-27	34.2841949	-5.1640849	26.40 ± 0.17	576 ± 139	-1.05 ± 0.30	8.01 ± 0.26
UDS-28	34.5002365	-5.1555958	25.89 ± 0.14	519 ± 100	-1.77 ± 0.21	8.01 ± 0.22
UDS-29	34.2632675	-5.1521745	26.35 ± 0.13	1003 ± 150	-1.90 ± 0.11	7.57 ± 0.21
UDS-30	34.4777718	-5.1475210	25.66 ± 0.14	533 ± 103	-0.65 ± 0.21	8.50 ± 0.22
UDS-31	34.2963257	-5.1444168	25.95 ± 0.12	546 ± 88	-2.17 ± 0.14	7.81 ± 0.20
UDS-32	34.4192429	-5.1428924	25.83 ± 0.12	721 ± 138	-1.69 ± 0.21	7.91 ± 0.22
UDS-33	34.2468109	-5.1391201	26.06 ± 0.11	553 ± 85	-1.54 ± 0.19	7.99 ± 0.20
UDS-34	34.3719330	-5.1372724	24.83 ± 0.05	586 ± 50	-2.73 ± 0.08	8.01 ± 0.17
UDS-35	34.3146935	-5.1336756	26.42 ± 0.21	1125 ± 315	-1.20 ± 0.28	7.80 ± 0.28
UDS-36	34.2617569	-5.1346722	25.32 ± 0.08	658 ± 76	-2.16 ± 0.12	7.97 ± 0.18
UDS-37	34.3805695	-5.2681055	26.54 ± 0.22	832 ± 249	-1.34 ± 0.28	7.71 ± 0.29
UDS-38	34.4414444	-5.2159638	26.60 ± 0.19	912 ± 208	-2.14 ± 0.14	7.38 ± 0.25
UDS-39	34.3348541	-5.1771636	26.99 ± 0.18	594 ± 145	-2.39 ± 0.24	7.26 ± 0.26
UDS-40	34.4380951	-5.1600704	26.86 ± 0.17	677 ± 157	-2.29 ± 0.21	7.30 ± 0.25

Note. — ID: running identification number prefixed by the respective field acronyms; RA/DEC: coordinates from the CANDELS catalogs; H : H -band AB magnitude from the CANDELS catalog; $EW_{\text{OIII},5007}$: rest-frame equivalent width inferred from the I , J , and H broad-band photometry (see text for details); β_{2500} : F_{λ} continuum slope at rest-frame 2500Å inferred from a linear fit to the B , V , and I broad-band photometry; $\log(M)$: stellar mass inferred from Starburst99 (Leitherer et al. 1999), as described in the text.

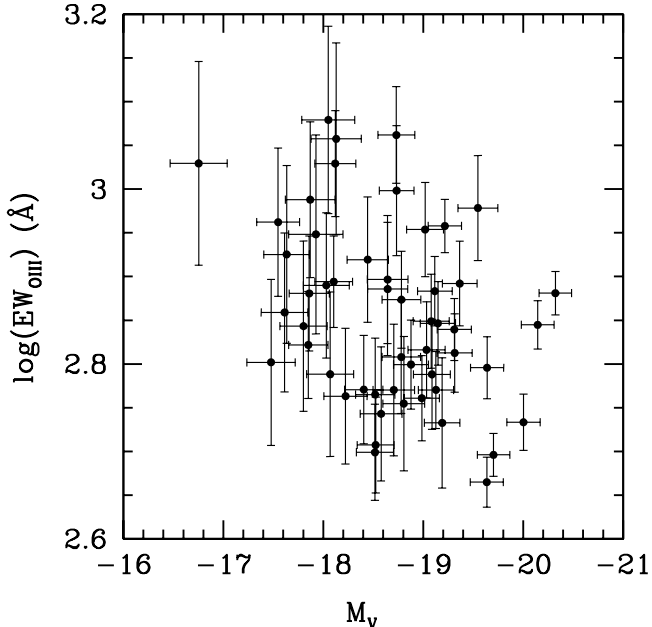


Figure 5. Rest-frame V-band luminosity vs. rest-frame equivalent width of the [OIII] emission line at 5007Å as calculated from the broad-band photometry as explained in the text and assuming that all emission-line galaxy candidates are at $z = 1.7$. They span a range in luminosity, $M_V = -17$ to $M_V = -20$, and have $EW_{[OIII],5007}$ between 500Å and 1200Å. See also Table 1.

most, when assuming an Eddington accretion of unity. At these low masses, at least at the present day, secular processes drive nuclear activity; thus, an as of yet unknown accretion mode or triggering mechanism for nuclear activity would have to be invoked in order to explain an extreme change in the relative numbers of AGN and starburst powered emission-line dominated objects. At these low masses, merging cannot account for this. The starburst hypothesis, on the other hand, places these objects in the realm of dwarf galaxies, and their physical and statistical properties are consistent with the abundances and masses of dwarf galaxies as we will discuss below.

Although nuclear activity cannot be ruled out entirely – and line-strength gradients in star forming $z \sim 2$ galaxies suggest that weak AGN may contribute to some extent (Trump et al., submitted) – we can safely assume that the observed emission lines are effectively dominated by star formation activity.

4.2. Starburst Ages and Masses

We now turn to interpreting the observations in the context of the Starburst99 model (SB99, Leitherer et al. 1999), which includes predictions for how the EWs of Hydrogen recombination line evolve over time. Therefore, our first task is to estimate $H\beta$ line strengths from the data. We attribute the excess light in the J band, compared to the continuum light measured in the I and H bands, to combined effect of emission lines in the J band. Thus, we compute the equivalent width as follows:

$$EW = \left(f_J - \frac{f_I + f_H}{2} \right) \frac{W_J}{1+z}$$

where $W_J = 2845\text{Å}$ is the effective width of the J-filter response curve, $z = 1.7$ to correct the observed EW to the rest frame, and f is the flux f_ν in the respective filters.

The relative contributions of the various emission lines is constrained by fitting Gaussian components to the 3 emission lines seen in the grism spectra shown in Figure 4. We only use the 3 UDS spectra as $H\beta$ is only marginally seen in the GSD spectrum. The emission line ratios are remarkably similar for all 3 objects: $H\beta$ contributes 1/8 to the total flux and $[OIII]_{5007}$ is 5 times stronger than $H\beta$, suggesting a very low metallicity. Because the flux is dominated by the $[OIII]_{5007}$ line and is therefore more directly related to our observations, we show their inferred EWs in Figure 5 (also see Table 1). However, we model the observations by fitting the inferred $H\beta$ EWs to the SB99 predictions. These are always assumed to be 5 times smaller than the $[OIII]_{5007}$ EWs. The unavoidable intrinsic scatter in this conversion is mimicked by propagating a generous factor two in the errors of the quantities we infer below.

$EW_{H\beta}$ is a sensitive age indicator, as it is quickly reduced once a stellar population gains in mass or the star formation activity diminishes. For a SB99 model with continuous star formation with a Chabrier (2003) IMF with a high-mass cut off at $100M_\odot$ and metallicity $0.2Z_\odot$ ²⁰ the $H\beta$ EWs imply that the galaxies in our sample typically have ages of 10 – 20 Myr (Figure 6). If we assume a single burst model instead, we infer ages 3 – 5 Myr; all formation histories with declining star formation rates produce ages that are bracketed by these two extremes. In general, we conclude that the ages of these galaxies range from 3 – 40 Myr, which includes the intrinsic range in age and the systematic uncertainty due to the unknown star formation history. In the following we use the results from the continuous star formation model, but using the instantaneous burst model, by virtue of the insensitivity of the mass estimates to the choice of star formation history, does not change our interpretation and conclusions.

Given age, the SB99 model predicts the V-band mass-to-light ratio, such that we can directly estimate the mass after deriving the V-band luminosity from the observed H band magnitude. We correct the luminosity and the derived mass estimate for extinction by comparing the continuum slope derived from the ACS photometry at rest-frame 2500Å, typically $\beta_{2500} \sim -2$ (see Table 1), with the SB99 model prediction (rather constant at $\beta_{2500} \sim -2.6$ for the ages of these bursts). If we adopt the Calzetti et al. (2000) extinction law for starbursting galaxies the typical extinction is $E(B - V) = 0.2$.

The average burst mass is $8 \times 10^7 M_\odot$ (see Table 1 and Figure 6). Mass estimates inferred from the instantaneous burst model are only slightly smaller, by less than 0.1 dex on average. Internal consistency lends our modeling approach strong credibility: given the inferred ages, masses, and extinction corrections, the SB99 model predicts dust-attenuated rest-frame UV luminosities that are consistent with the observed rest-frame UV luminosities.

²⁰ The results also do not change significantly if we adopt a different model metallicity, but we do suffer from the usual, unknown uncertainty due to our lack of knowledge of the stellar IMF, especially at the high-mass end.

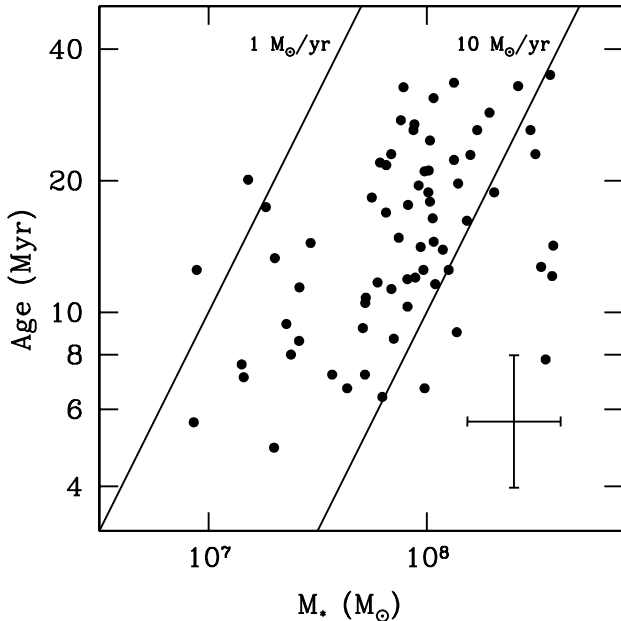


Figure 6. Masses, ages and star formation rates for the 69 emission-line dominated objects in our sample, derived with the SB99 model, assuming that all are at $z = 1.7$. We use the EW derived from the broad-band photometry as age indicator, adopting a continuous SF model with 0.2 times solar metallicity and a Salpeter IMF. The absolute V-band luminosity is then used to infer the total mass of the young starburst. The SFRs indicated by the diagonal lines are simply obtained by dividing the mass (x-axis) by the age (y-axis). Our modeling is described in more detail in the text. The galaxies in our sample typically have $10^8 M_{\odot}$ stellar masses with young ages (5 – 30 Myr), or, equivalently, extremely high specific SFRs ($\sim 5 \times 10^{-8} \text{ yr}^{-1}$, or $\sim 50 \times \text{Hubble}^{-1}$).

ties – the latter are not used in our modeling model. Thus, the model successfully describes the observed rest-frame UV and optical continuum spectral energy distributions as well as the observed emission line luminosities.

Full modeling of the spectral energy distributions that includes emission line contributions will be presented in forthcoming studies that will also include objects with less prominent emission lines. As a consistency check with the results presented above we already applied the method outlined by Finkelstein et al. (2011), which includes a photometric redshift determination, to the galaxies in our sample. We find photometric redshifts that are consistent with $1.6 < z < 1.8$ for the vast majority of the sample. Moreover, the inferred stellar masses and ages are very similar, even though this model is based on a different stellar population synthesis model (CB07 Bruzual & Charlot 2003).

The observed IRAC fluxes at $3.6\mu\text{m}$ and $4.5\mu\text{m}$ are in most cases – there are two exceptions – fully consistent with the expected fluxes for the bursts observed in the UV. In addition, the galaxies have the same sizes in the J and H bands, indicating that the spatial extent of the region from which the line emission originates roughly follows the stellar light. Hence, there is no evidence for underlying older stellar populations. However, we cannot rule out their existence: maximally old stellar populations have mass-to-light ratios that are up to ~ 50 times larger than those of the bursts, even in the near infrared.

If we assume a past star formation rate that is constant after averaging over > 100 Myr time scales we find upper limits for the mass in older stars that is $\sim 5 \times$ the burst mass. The implied total stellar mass upper limits are then $\sim 5 \times 10^8 M_{\odot}$. This caveat notwithstanding, we assume in the remainder of this paper that there is no significant population of older stars in these galaxies, and that the observed bursts account for the total stellar mass. However, the bottom line is that the total stellar masses of these objects are well below $10^9 M_{\odot}$, in the regime of dwarf galaxies.

4.3. Gas Content and Energy Budget

The most remarkable property of these galaxies are their growth rates (specific star formation rates) of $20 - 200 \text{ Gyr}^{-1}$. This is far outside the realm of normal star forming galaxies. The SFR and the sizes of the galaxies ($\sim 0.5 \text{ kpc}$), together with the inverted Schmidt-Kennicutt law (Schmidt 1959; Kennicutt 1998; Genzel et al. 2011), imply total gas masses of order $10^9 M_{\odot}$, or gas fractions of $f_g \sim 0.9$.

Given these reservoirs of gas, the observed level of star formation could in principle be fueled for much longer periods of time, up to a few times 10^8 yr . However, the amount of energy deposited into the gas through winds and supernovae exceeds the binding energy of the gas by an order of magnitude, which implies that the gas may be in the process of being blown out, ending the starburst. Another possible consequence of the large amount of injected energy over a short period of time is that this may provide a mechanism to produce cored profiles for the dark matter halos of low-mass galaxies. Alternatively, if all the gas is expelled, then the stars would become unbound as well, dissolving the entire stellar body. These speculative scenarios can be tested further with better observational constraints on the gas masses and hydrodynamical modeling of these systems.

Besides considering the truncation of the observed starburst events after a relatively brief period, an interesting puzzle is what causes or regulates the onset of these starburst in the first place. Simulations indicate a natural semi-periodic star formation history for low-mass galaxies. Alternatively, it may be that star formation had been suppressed at earlier epochs as a result of UV background radiation (e.g., Babul & Rees 1992; Babul & Ferguson 1996), although this is generally thought to play a role only at even lower masses.

5. DISCUSSION: COSMOLOGICAL CONTEXT

5.1. Comparison with Other Samples

Galaxies with similar properties have previously been identified through broad-band photometry at $z < 0.4$ in the Sloan Digital Sky Survey (Cardamone et al. 2009), and have been shown by Izotov et al. (2011) to constitute the most strongly star-forming tail of the well-known class of blue compact dwarf galaxies (e.g., Sargent & Searle 1970; Thuan & Martin 1981), which have very low metallicities and extremely high, spatially concentrated star-formation activity (Guzman et al. 1998; Overzier et al. 2008).

Cowie et al. (2011) (also see Scarlata et al. 2009) recently studied the Ly α properties of high-EW Ha emitters, providing a direct connection between higher-

redshift searches of Ly α (e.g., Ouchi et al. 2008; Hu et al. 2010), and find Ly α EWs ranging from 20Å to 200Å. Combining this with the findings of Nilsson et al. (2011), who show that Ly α emitters at $z \sim 2$ are objects with a very wide range in properties, it is clear that from Ly α emitters one cannot derive a complete description of star formation in low-mass galaxies. On the other hand, Ly α emitters at higher redshifts ($z > 3$) appear to be generally young, with small stellar masses (e.g., Finkelstein et al. 2009), similar to the emission line galaxies studied here. Atek et al. (2010) pointed out the existence of a class of emission line galaxies at $z \sim 1.5$ with EW $> 1000\text{\AA}$ that would most likely be included in our sample as well. However, so far, their nature has not been described and their cosmological relevance in the context of galaxy formation has remained unclear. Therefore, let us now put these starbursting dwarf galaxies in a cosmological context.

5.2. Implications for the Formation of Dwarf Galaxies

Our sample with redshifts $1.6 < z < 1.8$ consists of 69 low-mass ($\sim 10^8 M_\odot$), young ($\sim 0.5\text{--}4 \times 10^7$ yr), extreme starbursting, presumably metal-poor galaxies. Their co-moving number density²¹ is $3.7 \times 10^{-4} \text{ Mpc}^{-3}$, which is two orders of magnitude more than that of nearby galaxies with similar EWs (Cardamone et al. 2009). The star formation and number density combine into $1.7 \times 10^{-3} M_\odot \text{ yr}^{-1} \text{ Mpc}^{-3}$, a contribution of $\sim 2\%$ to the total star-formation rate density at $z \sim 1.7$ (e.g., Karim et al. 2011).

Unfortunately, we cannot constrain the number density of the general population of equally massive dwarf galaxies at $z \sim 1.7$: such objects will be at least 2 magnitudes fainter than the starbursting dwarf galaxies, and with marginal detections, even in the latest WFC3 data, and no obvious spectral features, their redshifts cannot easily be estimated. However, based on a reasonable and testable assumption that the observed bursts occur equally frequently at all epochs $1 < z < 3.5$ – a period of ~ 4 Gyr during which the cosmic star formation history peaked and after which the number density of starbursts drops as mentioned above – we can constrain the importance of the observed bursts for the formation of low-mass galaxies. The basic indication that such bursts are important is that the number of stars produced in such bursts over a period of several Gyr is comparable to the number stars that live in present-day dwarf galaxies.

In the following we put this on more quantitative footing by means of a simple model based on the observed quantities presented here and the mass function of present-day low-mass galaxies from Guo et al. (2011), who use the data from Baldry et al. (2008) for the galaxies with masses down to $10^7 M_\odot$. The Guo et al. (2011) mass function can be represented by a simple power law for all galaxies with masses $< 10^{10} M_\odot$, that is, well below the knee of the Schechter function:

$$\frac{\phi(M_*)}{\text{Mpc}^3 \text{ dex}(M)} \sim 0.043 \left(\frac{M_*}{10^8 M_\odot} \right)^{-0.37}.$$

Let us then express the mass of a present-day descen-

dant in terms of the following star formation history:

$$M_{\text{desc}} = \frac{M_{\text{burst}} \times N_{\text{burst}}}{f_{\text{burst}}},$$

where $M_{\text{burst}} \sim 2 \times 15 \text{ Myr} \times 5 M_\odot \text{ yr}^{-1} = 1.5 \times 10^8 M_\odot$ is the total mass produced in a single starburst (the factor 2 is included to convert the observed burst age to its total duration), N_{burst} is the number of bursts that occurs in each galaxy over the ~ 4 Gyr period, and f_{burst} is the fraction of the total stellar mass that is produced in such bursts. The co-moving number density of descendants with mass M_{desc} can be written as

$$\frac{\phi(M_{\text{desc}})}{\text{Mpc}^3 \text{ dex}(M)} \sim \frac{\phi_{\text{burst}}}{N_{\text{burst}}} \times \frac{4 \text{ Gyr}}{30 \text{ Myr}},$$

where ϕ_{burst} is the co-moving number density of the bursts observed at $z \sim 1.7$ (see above), and the duty cycle of $\sim 0.75\%$ has been explicitly included and is due to the adopted ~ 4 Gyr period over which the bursts occur combined with the total burst duration ($2 \times 15 \text{ Myr}$).

By equating $\phi(M_{\text{desc}})$ and $\phi(M_*)$ we see that the mass of the descendant, M_{desc} (and also the number of bursts, N_{burst}) is uniquely determined once f_{burst} (or N_{burst}) is fixed:

$$\frac{M_{\text{desc}}}{10^8 M_\odot} \sim 2.4 f_{\text{burst}}^{-1.6}.$$

Thus, in the case that f_{burst} is close to unity, that is, almost all stars are formed in bursts, we infer that each galaxy must undergo one or two bursts on average and that, therefore, $M_{\text{desc}} \sim M_{\text{burst}}$. It is perhaps more realistic to adopt a smaller value for f_{burst} . If $f_{\text{burst}} \sim 0.5$, we find that two or three bursts must occur in each galaxy, producing descendants with masses $\sim 10^9 M_\odot$. The latter would imply a growth in stellar mass between $z \sim 1.7$ and the present by at least a factor 3 given the mass constraints on the underlying populations of the observed starburst galaxies. Simulations suggest that the typical growth is indeed a factor of 3 or 4, but we should bear in mind that these simulations do not reproduce the observed co-moving number density evolution of low-mass galaxies with redshift (e.g., Guo et al. 2011). Therefore, these predictions should be treated with care.

Choosing f_{burst} very low (~ 0.1) implies a very large growth in mass, with high-mass descendants ($> 10^{10} M_\odot$). Such growth is unlikely; models are better observationally constrained for these higher masses and the prediction is that none of such massive galaxies undergo such strong evolution. Given these constraints, the general conclusion we can draw is that our observations suggest that many or most stars in present-day dwarf galaxies (with masses $> 10^9 M_\odot$) have formed in a small number of starbursts at $z > 1$. The main assumption is that the observed bursts do not only occur at $z = 1.6\text{--}1.8$, but are equally frequent over a much broader redshift range ($1 < z < 3.5$). It is straightforward to test this observationally.

5.3. Summary

Our discovery of an abundant population of low-mass galaxies at $z \sim 1.7$ with very strong emission lines provides strong evidence for the burst-like nature of star

²¹ the values for our two widely separate fields, UDS and GSD, differ by only 12%

formation activity in dwarf galaxies at $z > 1$. We propose that we have observed an important formation mode for dwarf galaxies in general: a small number of strong starbursts that occur at early epochs ($z > 1$) each form $\sim 10^8 M_{\odot}$ in stars in a very short time span (~ 30 Myr) to build up the bulk of the stellar components of present-day dwarf galaxies. This is in quantitative agreement with 'archaeological' studies of present-day dwarf galaxies, which have shown that their star formation histories are burst-like and that the ages of their stellar populations suggest formation redshifts $z > 1$ (e.g., Weisz et al. 2011). Our observations provide direct evidence for such an early formation epoch and, in particular, that short-lived bursts contribute much or even the majority of star formation in dwarf galaxies.

A.v.d.W. thanks those people who contributed to this paper through useful discussions, including Knud Jahnke, Brent Groves, Dan Weisz, Joe Hennawi, Kate Rubin, Sharon Meidt, and Marijn Franx

REFERENCES

- Atek, H., et al. 2010, *ApJ*, 723, 104
 Babul, A., & Ferguson, H. C. 1996, *ApJ*, 458, 100
 Babul, A., & Rees, M. J. 1992, *MNRAS*, 255, 346
 Baldry, I. K., Glazebrook, K., & Driver, S. P. 2008, *MNRAS*, 388, 945
 Bertin, E., & Arnouts, S. 1996, *A&AS*, 117, 393
 Bouwens, R. J., Illingworth, G. D., Franx, M., & Ford, H. 2008, *ApJ*, 686, 230
 Bruzual, G. & Charlot, S. 2003, *MNRAS*, 344, 1000
 Calzetti, D., Armus, L., Bohlin, R. C., Kinney, A. L., Koornneef, J., & Storchi-Bergmann, T. 2000, *ApJ*, 533, 682
 Calzetti, D., Meurer, G. R., Bohlin, R. C., Garnett, D. R., Kinney, A. L., Leitherer, C., & Storchi-Bergmann, T. 1997, *AJ*, 114, 1834
 Cardamone, C., et al. 2009, *MNRAS*, 399, 1191
 Chabrier, G. 2003, *PASP*, 115, 763
 Cowie, L. L., Barger, A. J., & Hu, E. M. 2011, arXiv:1106.0496
 Dolphin, A. E., Weisz, D. R., Skillman, E. D., & Holtzman, J. A. 2005, arXiv:astro-ph/0506430
 Finkelstein, S. L., Rhoads, J. E., Malhotra, S., & Grogin, N. 2009, *ApJ*, 691, 465
 Finkelstein, S. L., et al. 2011, *ApJ*, 729, 140
 Genzel, R., et al. 2011, *ApJ*, 733, 101
 Giavalisco, M., et al. 2004, *ApJ*, 600, L93
 Grebel, E. K. 1997, *Reviews in Modern Astronomy*, 10, 29
 Grogin, N. A., et al. 2011, arXiv:1105.3753
 Guo, Q., et al. 2011, *MNRAS*, 413, 101
 Guzman, R., Jangren, A., Koo, D. C., Bershad, M. A., & Simard, L. 1998, *ApJ*, 495, L13
 Harris, J., Calzetti, D., Gallagher, J. S., III, Smith, D. A., & Conselice, C. J. 2004, *ApJ*, 603, 503
 Häussler, B., et al. 2007, *ApJS*, 172, 615
 Hu, E. M., Cowie, L. L., Barger, A. J., Capak, P., Kakazu, Y., & Trouille, L. 2010, *ApJ*, 725, 394
 Hu, E. M., Cowie, L. L., Kakazu, Y., & Barger, A. J. 2009, *ApJ*, 698, 2014
 Ilbert, O., et al. 2010, *ApJ*, 709, 644
 Izotov, Y. I., & Thuan, T. X. 2008, *ApJ*, 687, 133
 Izotov, Y. I., Guseva, N. G., & Thuan, T. X. 2011, *ApJ*, 728, 161
 Kakazu, Y., Cowie, L. L., & Hu, E. M. 2007, *ApJ*, 668, 853
 Karim, A., et al. 2011, *ApJ*, 730, 61
 Kennicutt, R. C., Jr. 1998, *ARA&A*, 36, 189
 Koekemoer, A. M., et al. 2011, arXiv:1105.3754
 Labbé, I., et al. 2010, *ApJ*, 716, L103
 Laidler, V. G., et al. 2007, *PASP*, 119, 1325
 Lee, J. C. 2008, *Formation and Evolution of Galaxy Disks*, 396, 109
 Lee, J. C., Kennicutt, R. C., José G. Funes, S. J., Sakai, S., & Akiyama, S. 2009, *ApJ*, 692, 1305
 Leitherer, C., et al. 1999, *ApJS*, 123, 3
 Mas-Hesse, J. M., & Kunth, D. 1999, *A&A*, 349, 765
 Marchesini, D., van Dokkum, P. G., Förster Schreiber, N. M., Franx, M., Labbé, I., & Wuyts, S. 2009, *ApJ*, 701, 1765
 Mateo, M. L. 1998, *ARA&A*, 36, 435
 McLure, R. J., Dunlop, J. S., Cirasuolo, M., Koekemoer, A. M., Sabbi, E., Stark, D. P., Targett, T. A., & Ellis, R. S. 2010, *MNRAS*, 403, 960
 McQuinn, K. B. W., Skillman, E. D., Cannon, J. M., Dalcanton, J. J., Dolphin, A., Stark, D., & Weisz, D. 2009, *ApJ*, 695, 561
 Nagamine, K. 2010, *Advances in Astronomy*, 2010, 16
 Nilsson, K. K., Östlin, G., Möller, P., Möller-Nilsson, O., Tapken, C., Freudling, W., & Fynbo, J. P. U. 2011, *A&A*, 529, A9
 Oesch, P. A., et al. 2010, *ApJ*, 709, L16
 Ono, Y., Ouchi, M., Shimasaku, K., Dunlop, J., Farrah, D., McLure, R., & Okamura, S. 2010, *ApJ*, 724, 1524
 Ouchi, M., et al. 2008, *ApJS*, 176, 301
 Overzier, R. A., et al. 2008, *ApJ*, 677, 37
 Pelupessy, F. I., van der Werf, P. P., & Icke, V. 2004, *A&A*, 422, 55
 Salzer, J. J., Rosenberg, J. L., Weisstein, E. W., Mazzarella, J. M., & Bothun, G. D. 2002, *AJ*, 124, 191
 Sargent, W. L. W., & Searle, L. 1970, *ApJ*, 162, L155
 Scarlata, C., et al. 2009, *ApJ*, 704, L98
 Schaerer, D., Contini, T., & Kunth, D. 1999, *A&A*, 341, 399
 Schaerer, D., & de Barros, S. 2009, *A&A*, 502, 423
 Schmidt, M. 1959, *ApJ*, 129, 243
 Shen, Y., Greene, J. E., Strauss, M. A., Richards, G. T., & Schneider, D. P. 2008, *ApJ*, 680, 169
 Springel, V., et al. 2005, *Nature*, 435, 629
 Straughn, A. N., et al. 2008, *AJ*, 135, 1624
 Straughn, A. N., et al. 2009, *AJ*, 138, 1022
 Straughn, A. N., et al. 2011, *AJ*, 141, 14
 Thornley, M. D., Schreiber, N. M. F., Lutz, D., Genzel, R., Spoon, H. W. W., Kunze, D., & Sternberg, A. 2000, *ApJ*, 539, 641
 Thuan, T. X., & Martin, G. E. 1981, *ApJ*, 247, 823
 Tremonti, C. A., Calzetti, D., Leitherer, C., & Heckman, T. M. 2001, *ApJ*, 555, 322
 Weisz, D. R., et al. 2011, arXiv:1101.1093
 Windhorst, R. A., et al. 2011, *ApJS*, 193, 27